Available online at www.sciencedirect.com

SciVerse ScienceDirect

Ceramics International 39 (2013) 3077–3086

CERAMICS INTERNATIONAL

www.elsevier.com/locate/ceramint

Effect of sintering temperature on electromagnetic properties of NiCuZn ferrite

Ch. Sujatha[a,*], K. Venugopal Reddy[a], K. Sowri Babu[a], A. RamaChandra Reddy[a], K.H. Rao[b]

[a]*Department of Physics, National Institute of Technology, Warangal 506004, Andhra Pradesh, India*
[b]*Department of Physics, RGU-IIIT, Nuzvid 521201, Andhra Pradesh, India*

Received 6 June 2012; received in revised form 25 September 2012; accepted 26 September 2012
Available online 8 October 2012

Abstract

$Ni_{0.50}Cu_{0.05}Zn_{0.45}Fe_2O_4$ ferrite nanoparticles were processed through the sol–gel method using polyvinyl alcohol as a chelating agent. The dried powder after annealing (500 °C for 3 h) was compacted and sintered at three different temperatures (900, 950 and 1030 °C) for 1 h. In this article, optimum sintering temperature required for NiCuZn ferrite system, for obtaining good electromagnetic properties, suitable for Multilayer Chip Inductor (MLCIs) applications was studied. The structural, magnetic and dielectric properties were investigated as a function of sintering temperature. X-ray diffraction patterns for the sintered samples confirmed formation of single phase cubic spinel structure. Microstructure and grain size distribution for the samples were investigated by FESEM which displayed homogeneous grains of polyhedral shape by retaining almost temperature independent grain shape but with increased grain size along with the increase of sintering temperature. Saturation magnetization showed increasing trend with sintering temperature up to 950 °C and decreased after that. The sample sintered at 950 °C exhibited low magnetic losses, high saturation magnetization and high frequency stability of permeability with cut off frequency around 30 MHz.

Keywords: A. Sintering; C. Dielectric properties; C. Magnetic properties; D. Spinels

1. Introduction

Recently, surface mounting devices (SMD) have been rapidly developed for electronic applications, such as multilayer chip inductors (MLCIs).These are produced by coating ferrite and silver (Ag) electrode layers alternately and then co-firing them [1]. The main requirements of MLCIs are good quality factor; high electrical resistivity; high magnetic permeability for reducing number of layers thereby minimizing the capacity between the layers and hence realizing the miniaturization [2,3]. Besides that, low sintering temperature is necessary for avoiding diffusion of Ag (<961 °C melting point of Ag) into the ferrites which adversely affect the electrical resistivity [4]. NiZn ferrite has wide application prospect in the field of RF electron devices due to high permeability in combination with giant resistivity but at the same time it requires high sintering temperature for densification [5]. Recently there is a growing interest on NiCuZn ferrites for MLCIs applications because these oxides can be sintered at relatively low temperatures and also these materials exhibit good electromagnetic properties at higher frequencies [6,7]. In addition to that, it has better magnetic properties at high frequencies than MnZn ferrites and lower densification temperatures than NiZn ferrites [8]. Even though small amount of Cu substituted in NiZn bulk ferrites still require high sintering temperature (≥ 1000 °C) with longer duration of soaking time (for densification) which in turn cause evaporation of some of the constituents and also consumes more power [9]. Also the conventional method of preparation does not ensure neither stoichiometry nor homogeneity [10]. Thus, to reduce the sintering temperature there are several techniques that exist: (1) Synthesis of active ultra fine powders by wet chemical routes and (2) use of sintering aids [11]. The first one is better than the other because after a critical concentration of sintering aids, they are separated

*Corresponding author. Tel.: +91 870 2462560; Mob.: +91 9502899683; fax: +91 870 2459547.
E-mail address: sujatha.phys09@gmail.com (Ch. Sujatha).

0272-8842/$ - see front matter © 2012 Elsevier Ltd and Techna Group S.r.l. All rights reserved.
http://dx.doi.org/10.1016/j.ceramint.2012.09.087

from the lattice and form secondary phase at the grain boundary. This causes deterioration of electromagnetic properties of the ferrites.

Sun et al. [12] studied the effect of iron deficient, excess iron and stoichimetric NiCuZn ferrite systems on phase formation, grain size and magnetic properties. They reported that stoichiometric NiCuZn ferrite possess highest magnetization, permeability and lowest core losses compared to other systems. Caltun et al. [13] investigated both the effect of doping and sintering temperature on permeability spectra of NiZn ferrite and found that addition of small amount of CuO decreases the sintering temperature and improves the high frequency performance. With sintering temperature the permeability changes depending on the microstructure of the sample. Penchal Reddy et al. [14] investigated $Ni_{0.4-x}Cu_{0.05}Zn_{0.55+x}Fe_2O_4$ ferrite prepared through microwave sintering method with low sintering temperature (950 °C) and observed that the composition $Ni_{0.3}Cu_{0.05}Zn_{0.65}Fe_2O_4$ showed highest magnetization and permeability. There are literature reports stating that variations in the heat treatment conditions such as calcination temperature, heating rate and sintering temperature influence the permeability spectra as well as resonance frequency [15,16]. Ghodake et al. [6] studied NiCuZn ferrite system with various compositions prepared through oxalate precursor method and sintered at 1000 °C for 6 h which exhibited better magnetic properties. For optimizing the sintering conditions along with the improvement of magnetic properties suitable for MLCIs applications, the composition $Ni_{0.5}Cu_{0.05}Zn_{0.45}Fe_2O_4$ was chosen from the above mentioned report. These materials were processed through sol–gel technique which facilitates greater homogeneity and uniform particle size distribution. A small percent of Cu substitution in place of Zn in NiZn ferrite is advantageous to improve initial permeability and also to reduce sintering temperature which indirectly avoids Zn evaporation and so leads to increase of electrical resistivity. In the present paper electromagnetic properties of NiCuZn ferrite system was studied as function of sintering temperature.

2. Experimental

In order to prepare $Ni_{0.50}Cu_{0.05}Zn_{0.45}Fe_2O_4$ ferrite, analytical grade nickel nitrate, zinc nitrate, copper nitrate and ferric nitrate were dissolved separately in minimum amount of deionised water in the required stoichiometric proportions. The formed cationic solutions were mixed together and stirred for 1 h to improve homogeneity; the resulting solution was known as precursor. The molar ratio of total metal ions to polyvinyl alcohol (PVA) was maintained at 1:3.The PVA, in measured quantity, was added to the precursor and dehydrated around 100 °C under continuous stirring. The gelation continued step by step till a slightly red gel type product was formed with the release of reddish brown gases around 100 °C, where the gel further got converted into a fluffy ferrite mass which was annealed at 500 °C for 3 h to remove PVA. The annealed powder was ground in agate mortar and mixed with 15% of PVA as binder for making disk shaped pellets and toroids. These were sintered at temperatures of 900 °C, 950 °C and 1030 °C for 1 h with a heating rate of 5 °C/min in a programmable muffle furnace.

2.1. Characterization

The sintered samples were characterized by X-ray diffraction using Inel X-ray diffractometer (XRG 3000) equipped with Co-Kα ($\lambda = 1.78897$ Å) radiation source to examine the phase and structure. The microstructure and selected area diffraction patterns of the annealed sample were obtained using High Resolution Transmission Electron Microscope (HRTEM). Thermal decomposition behavior of the dried gel was examined by means of Differential Scanning Calorimeter (DSC Q9 V9.6 TA) with a heating rate of 10 °C/min. The Fourier Transform Infrared (FTIR) spectra recorded on Shimadzu 820/PC in the wave number region from 4000 to 400 cm^{-1} using KBr pellet method. Morphology and grain size distribution of nanoparticles were investigated by field emission scanning electron microscope (FESEM) Carl Zeiss Ultra 55 operating at an accelerating high tension voltage EHT of 17 kV. Vibration sample magnetometer (EV-7 VSM) was used to measure room temperature saturation magnetization (M_s) and intrinsic coercive force (H_c) in an applied field of 20 kOe. Dielectric properties were measured using HP4192 A LF Impedance analyzer. Permeability measurements were carried out on the toroid samples using High frequency LCR meter (WAYNKERR 6500 P) operating in the frequency range of 100 Hz–50 MHz. The initial permeability was calculated using the observed and air core inductance

$$\mu_i = \frac{L}{L_o}$$

where L is the observed inductance in μH and L_o is the air core inductance

$$L_o = 0.004606 N^2 h \log\left(\frac{OD}{ID}\right) 10^{-6}$$

where N is the number of turns, h is the thickness of the toroid in inches and OD, ID are the outer and inner diameters of the toroid.

3. Results and discussion

3.1. Structural analysis

X-ray diffraction patterns (Fig. 1) of the sintered samples showed single phase cubic spinel structure. The well resolved peaks in the XRD pattern clearly indicate polycrystalline nature of the ferrites and are similar to JCPDS card No. 08-0234. In nanomaterials, both the crystallite size and lattice strain are known to have their

own contributions to the X-ray diffraction peak broadening. According to diffraction theory, peak broadening due to crystallite size, varies as sec θ and strain as tan θ [17]. The accurate crystallite size was estimated using Williamson–Hall (W–H) analysis since it differentiates size induced and strain induced peak broadening by considering the peak width as a function of 2θ [18]. The crystallite size calculated using Debye-Scherrer's formula after eliminating the instrumental broadening effect is

$$D = \frac{0.9\lambda}{\beta \cos\theta}$$

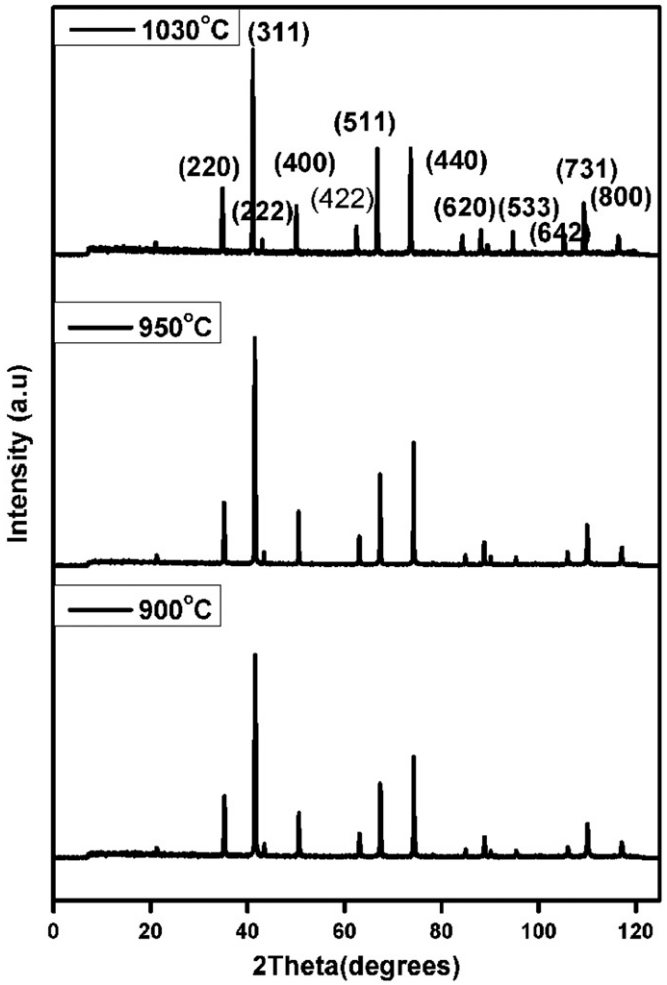

Fig. 1. XRD patterns for $Ni_{0.50}Cu_{0.05}Zn_{0.45}Fe_2O_4$ ferrite sintered at 900 °C, 950 °C and 1030 °C.

where $\beta = \sqrt{(\beta^2_{Measured} - \beta^2_{instrumental})}$ is the peak broadening after removing the instrumental broadening, λ(1.78897 Å) is the wavelength of X-rays used and θ is the peak center. W–H equation for size and strain broadening [18] is

$$\beta \cos\theta = \frac{0.9\lambda}{D} + 4\varepsilon \sin\theta$$

A graph drawn between $\beta\cos\theta$ versus $4\sin\theta$ gives a straight line graph with a positive intercept and the reciprocal of the intercept gives crystallite size. Accurate estimation of lattice constant has been done using Nelson–Riley (NR) extrapolation method by minimizing both systematic and random error. The values of the lattice parameter obtained from each reflected plane were plotted against the NR function F(θ).

$$F(\theta) = \frac{1}{2}\left[\frac{\cos^2\theta}{\sin\theta} + \frac{\cos^2\theta}{\theta}\right]$$

A straight line graph was obtained [19]. The extrapolation of the straight line to F(θ)=0 or θ=90° gives an accurate lattice constant. The observed lattice constant, crystallite size, frequency bands (ν_1,ν_2), bulk density and magnetization data as a function of sintering temperature are shown in Table 1. The crystallite size increased with sintering temperature up to 950 °C and thereafter decreased, this may be due to the formation of secondary phase at higher temperature of sintering. The presence of trace amount of secondary phase (< 5%) in the sample sintered at 1030 °C is not identified in XRD. The bulk density of the disc shaped pellet was calculated by considering dimensions and weight of the sample

$$d_{Bulk} = \frac{mass}{\Pi r^2 t}$$

where r and t are the radius and thickness of the pellet. The density of the sintered samples improved with sintering temperature and is in the orders of 3.7672 g/cm^3.The bulk density is comparable to that of materials prepared through chemical route techniques such as sol–gel auto combustion [20] but lower than the other reports [4,6]. It is known fact that the material properties are dependent on the composition, preparation techniques and heat treatment conditions. This may be the reason for low values of density for the present samples compared to the literature reports [4,6].

Table 1
Crystallite size, lattice constant, saturation magnetization (M_s), coercivity (H_c), and ν_1, ν_2 frequency bands for the sintered samples.

Sintering temperature (°C)	Lattice constant (Å)	Crystallite size (nm)	Saturation magnetization M_s (emu/g)	Coercivity H_c (Oe)	ν_1 (cm^{-1})	ν_2 (cm^{-1})
900	8.3855	49	66.91	49	588	403
950	8.3859	63	76.67	33	590	407
1030	8.4131	41	72.73	12	582	405

3.2. Thermal analysis

Fig. 2 shows the DSC curve of the as prepared sample. An endothermic peak at 95 °C with a shoulder peak around 131 °C was observed. It corresponds to the elimination of physically adsorbed water; water with in the lattice and from the pores [21]. Further two exothermic peaks at 212 °C and 391 °C were found corresponding to combustion of un-reacted organic ligands and crystallization of spinel phase respectively. The toothed curve of DSC is due to release of water and formation of M–O–M (metal-oxygen-metal) bridges [21].

3.3. Microstructural analysis

Morphology and microstructure of the annealed sample was investigated by HRTEM. The microstructure, lattice fringe patterns of the nanoparticle and selected area electron diffraction pattern (SAED) of the annealed sample are as shown in Fig. 3. The morphology of the annealed samples showed fine spherical particles (Fig. 3(a)) and the particle size is in the range of 6–15 nm which is in agreement with the crystallite size (19 nm) determined by considering peak broadening of highest intensity (311) peak using Debye Scherrer's formula (inset of Fig. 3(a)). The SAED patterns in Fig. 3(c) confirms the crystalline nature of the annealed sample. From the fringe patterns (Fig. 3(b)) of the nanoparticle having particle size ~14 nm, it is confirmed that the crystal planes of one particular orientation (400) are confined within a particle, indicating that the particle is a single crystal with no defects [22]. The plane spacing d for the plane (400) calculated from lattice fringes is 0.212 nm which is coinciding with the standard d spacing of spinel phase.

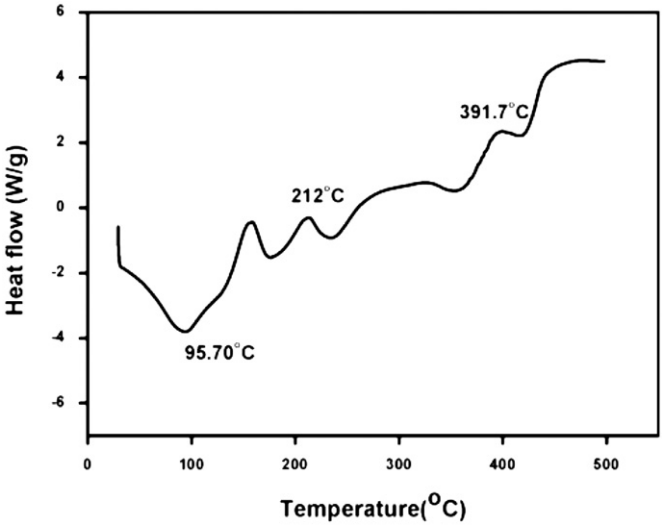

Fig. 2. DSC curve for the dried gel heated up to 500 °C.

FESEM microstructures of the samples sintered at 900,950 and 1030 °C are shown in Fig. 4(a), (b) and (c) respectively. All the samples displayed polyhedral morphology with uniform grains. The average grain sizes of all the samples were determined by counting a sufficiently large number of grains to ensure accuracy. The sample sintered at 900 °C exhibited well defined grain boundaries with intergranular porosity, having an average grain size of 104 nm. Whereas the sample sintered at 950 °C showed an increased grain size of 115 nm with reduced porosity. Larger grains were observed in the case of sample sintered at 1030 °C with an increased intact among the grains having an average grain size of 160 nm. The densification mechanism in ferrites is mainly due to diffusion of oxygen vacancies [23]. As pointed out in literature, at higher temperatures of sintering, Fe^{3+} ions were reduced to Fe^{2+} ions creating oxygen vacancies resulting in increased densification with larger grains [24]. Also Fe^{2+} ions diffuse very fast thereby grain growth takes place [25]. All these factors affecting the microstructure of the sample sintered at 1030 °C, resulting in enlarged grain size. The presence of Fe^{2+} ions at higher sintering temperature (1030 °C) was confirmed through FTIR spectra discussed in the next section.

3.4. FTIR analysis

FTIR spectrum for the sintered samples showed two strong frequency bands (ν_1, ν_2) around 600 and 400 cm^{-1} which correspond to characteristics of ferrites. The band ν_1 is assigned to the vibrations of the bond between the oxygen ion and the tetrahedral metal ion $O–M_{tetra}$ and the band ν_2 is assigned to the vibrations of the bond between

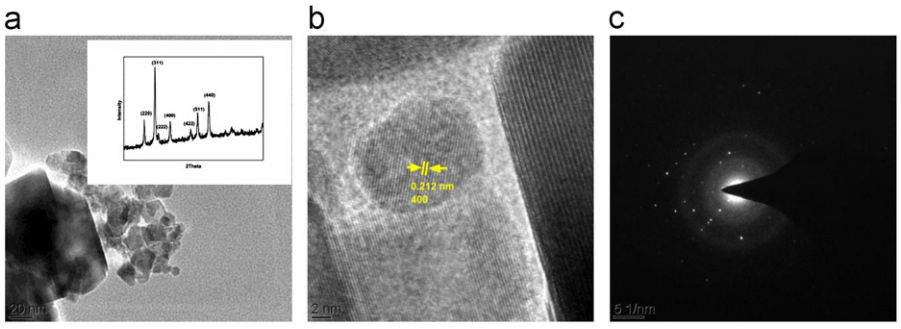

Fig. 3. HRTEM images of the $Ni_{0.50}Cu_{0.05}Zn_{0.45}Fe_2O_4$ ferrite annealed at 500 °C for 3 h (a) microstructure, (b) fringe pattern taken on a single particle and (c) SAED pattern of the particle.

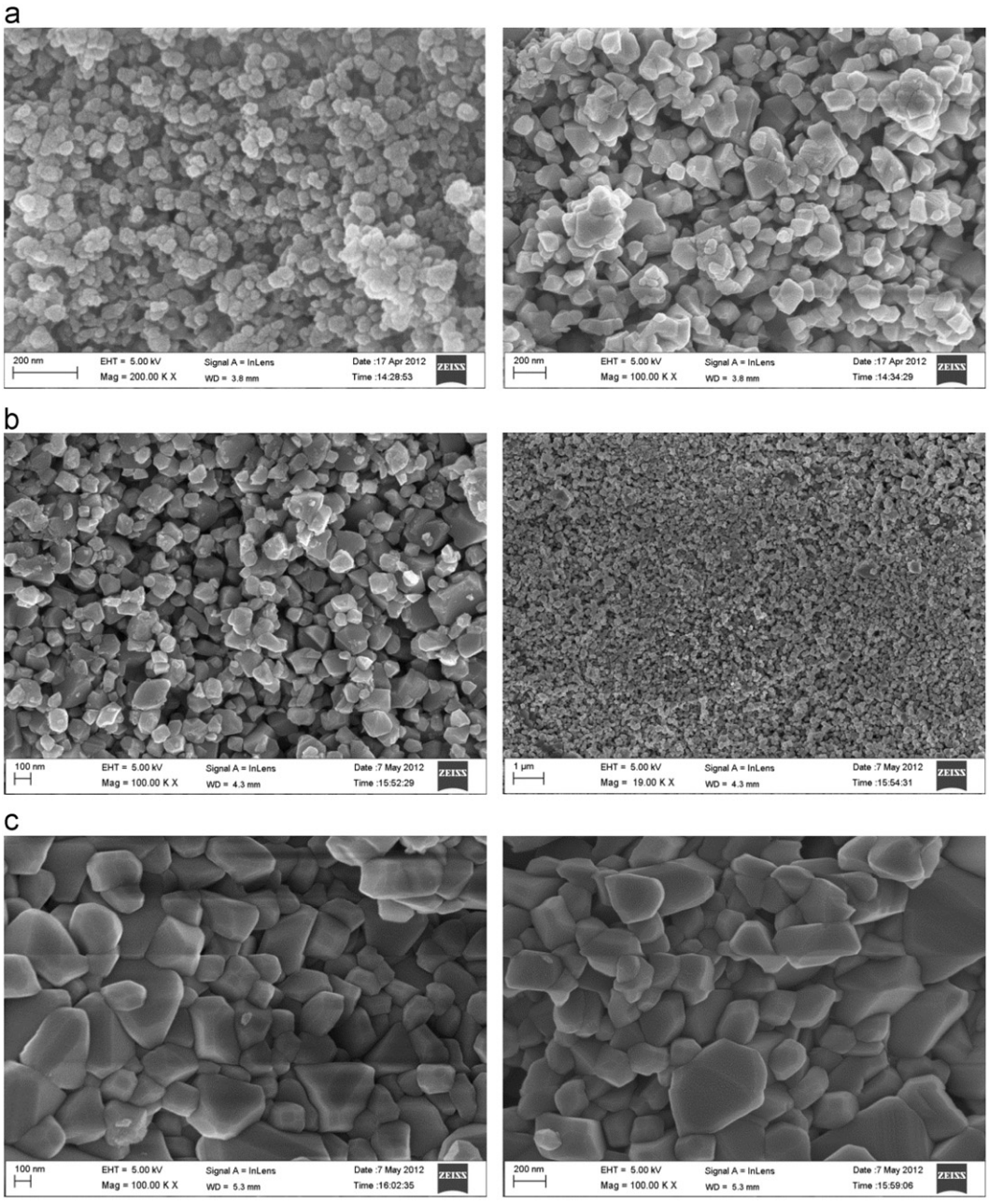

Fig. 4. FESEM micrographs for $Ni_{0.50}Cu_{0.05}Zn_{0.45}Fe_2O_4$ ferrite sintered at: (a) 900 °C (b) 950 °C and (c) 1030 °C.

the oxygen ion and the octahedral metal ion $O–M_{octa}$ [26]. The difference (Table 1) in the band positions were seen in the spectra due to the change in the bond length between $Fe^{3+}–O^{2-}$ ions for tetrahedral and octahedral complexes [27]. There is a slight variation in band positions of ν_1 and ν_2 as a function of sintering temperature since they are known to be affected by the method of preparation, grain size and heat treatment conditions [27]. In addition to these strong bands, there is a weak band observed around 470 cm^{-1} for the sample sintered at 1030° which is attributed to the presence of Jahn Teller Fe^{2+} ions in the sample (Fig. 5). The presence of these ions creates non cubic crystal field potential which causes splitting of the frequency bands [28]. The existence of Fe^{2+} ions is also confirmed through a basic test of red-ox titration of potassium dichromate using Barium salts of diphenylamine sulfonate as an indicator [29].

3.5. Room temperature magnetic properties analysis

Magnetic properties like saturation magnetization (M_s) is influenced by intrinsic factors such as preferential site occupancy of the cations, composition and is also influenced by extrinsic factors like microstructure and bulk density of the ferrites [30]. Room temperature hysteresis loops for the samples sintered at different temperatures are shown in Fig. 6. It is observed that M_s is increasing with sintering temperature up to 950 °C with maximum value of specific saturation magnetization M_s is 76.76 emu/g and

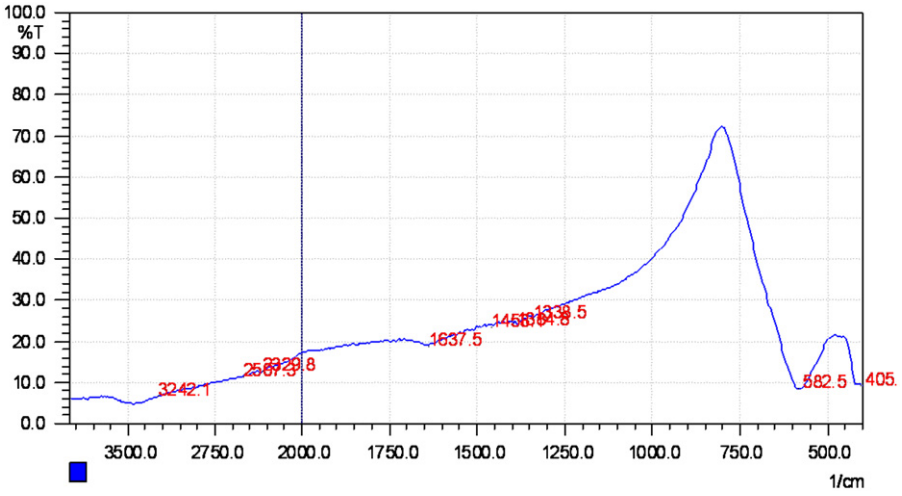

Fig. 5. FTIR spectra of $Ni_{0.50}Cu_{0.05}Zn_{0.45}Fe_2O_4$ ferrite sintered at 1030 °C.

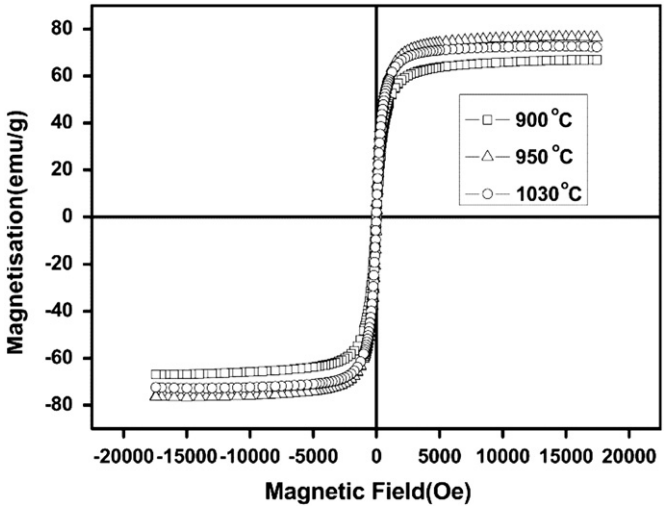

Fig. 6. Room temperature hysteresis loops for $Ni_{0.50}Cu_{0.05}Zn_{0.45}Fe_2O_4$ ferrite sintered at 900 °C, 950 °C and 1030 °C.

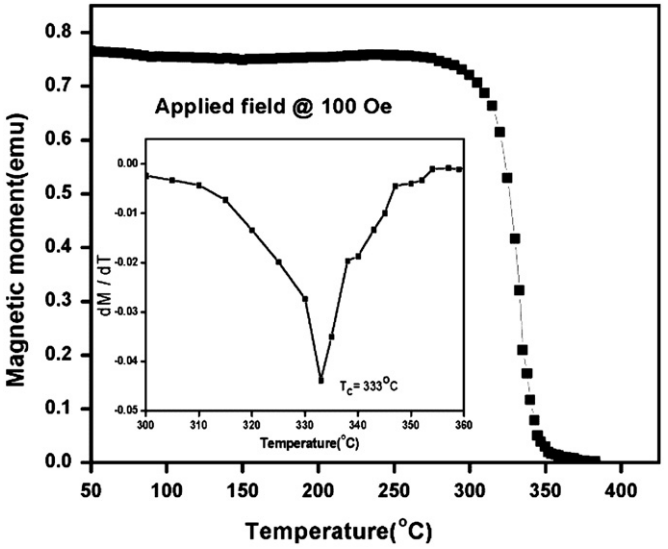

Fig. 7. Thermo magnetic curve for $Ni_{0.50}Cu_{0.05}Zn_{0.45}Fe_2O_4$ ferrite sintered at 950 °C. (Inset of the figure shows derivative of magnetic.moment with temperature).

decreases thereafter (Table1). The increased magnetization with sintering temperature (up to 950 °C) was attributed to improved grain size [20]. The decrease of M_s after the sintering temperature of 950 °C is due to Zn evaporation at higher sintering temperature resulting in the formation of excess antiferromagnetic hematite (α-Fe_2O_3) which is partly converted to magnetite (Fe_3O_4) [31]. Presence of antiferromagnetic hematite and $Fe^{2+}(4\mu_B)$ ions causes reduced magnetization. The intrinsic coercive force (H_c) showed decreasing trend with increasing sintering temperature. This indicates that particles are in multidomain (MD) state and in such a case the coercivity has inverse relationship with grain size (D). Coercivity varies linearly with anisotropy constant (K_1) and inversely with the grain size (MD). In the present case, influence of grain size on coercivity is predominant, there by corecivity decreased with increase of sintering temperature.

Fig. 7 shows thermo magnetic curve for the sample sintered at 950 °C. Temperature variation of magnetization provides the maximum temperature limit for the existence of ferrimagnetic ordering; beyond this temperature, transition from ferri to paramagnetic state takes place and it is about 333 °C for the sample sintered at 950 °C. Critical diameter for single domain particle was calculated using [32]:

$$D_c = \frac{9w_p}{2\pi M_s^2}$$

where w_p domain wall energy and is given by $w_p = (2k_B T_c K_v/a)^{(1/2)}$, M_s is the saturation magnetization, k_B is the Boltzmann constant, T_c is the Curie temperature, K_v is the magneto crystalline anisotropy constant and a is the lattice constant.

Multidomain or single domain nature of the particles is inferred from critical diameter which is calculated by making use of magneto crystalline anisotropy constant from the literature, near to our composition $K_1 = 3.65 \times 10^4$ erg/cm^3

[6]. Whereas the Curie temperature (T_c=606 K), magnetization (314 G) and lattice constant (a=8.3859 Å) are from the experimental observations. The critical diameter obtained is 39 nm which is lower than the grain size of the sintered samples observed from the FESEM micrographs indicating multidomain nature of the samples. Besides that low value of M_r/M_s ratio also validate the existence of multidomains.

3.6. Frequency dispersion of permeability spectra analysis

Frequency dispersion of permeability for the samples sintered at 900 °C, 950 °C and 1030 °C are as shown in Fig. 8. In general, permeability of a polycrystalline ferrite is related to two different magnetization mechanisms; spin rotational and domain wall magnetizations [33]. At lower frequencies, domain wall motion has major contribution to the permeability than spin rotation. The permeability due to domain wall motion is given by [34]:

$$(\mu_i)_{dw} \alpha \frac{M_s^2 D}{K_1}$$

where M_s is the saturation magnetization, D is the average grain size, and K_1 is the magneto crystalline anisotropy constant. It is known that initial permeability can be improved; either by selection of optimized chemical composition; by microstructures with high densities; by large grain sizes and thin grain boundaries [23]. Frequency dispersion of permeability spectra (Fig. 8) shows decreasing trend at low frequency and has maximum at higher frequency followed by a drop in the permeability. This is attributed to the mixed behavior of the type relaxation resonance phenomenon [35]. Permeability due to domain wall motion increased with sintering temperature due to improved grain size as discussed earlier. The increased permeability for the samples sintered at 900 and 950 °C is due to combined contributions of increased magnetization and grain size. In case of the sample sintered at 1030 °C the increase of permeability is due to increased grain size.

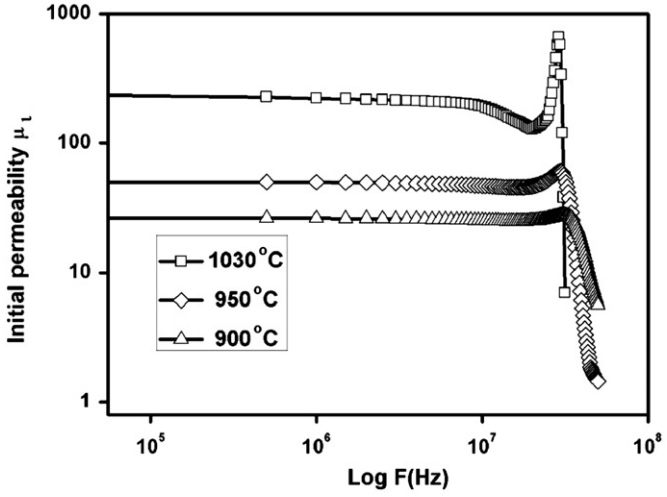

Fig. 8. Frequency dispersion of permeability spectra for $Ni_{0.50}Cu_{0.05}Zn_{0.45}Fe_2O_4$ ferrite sintered at 900 °C, 950 °C and 1030 °C.

The static permeability μ_i at 1 MHz for the samples sintered at 900 °, 950 °C and 1030 °C is 26, 49 and 222 respectively. The cut-off frequency for the samples sintered at 900 °C, 950 °C and 1030 °C is 31, 30 and 29 MHz respectively. With increasing sintering temperature, cut-off frequency decreased. Thus the present samples are in consensus with Snoek's law. The samples sintered at 900 °C and 950 °C exhibited flat profile of permeability with frequency up to 25 MHz, indicating compositional stability and quality of the material. The sample sintered at 1030 °C displayed frequency stability of permeability up to 8.5 MHz indicating increased dispersion of permeability with sintering temperature. Thus, samples exhibit constant permeability with frequency up to tens of MHz indicating large band width with an extended zone of utility (25 MHz) compared to the similar composition [6].

Quality factor (Q) for all the sintered samples increased with frequency (Fig. 9(a)) showing a peak and decreased thereafter due to ferrimagnetic resonance losses [36] and the sample sintered at 950 °C exhibited higher quality factor. In ferrite materials magnetic losses are due to phase lag of domain wall motion with respect to the applied AC magnetic field. The variation of magnetic loss factor (tanδ) with frequency (Fig. 9(b)) for the samples sintered at 900 °C and 950 °C showed high values at low frequencies and remains constant at higher frequencies. In case of sample sintered at 1030 °C, magnetic loss factor tanδ exhibited a peak around 10 MHz. It corresponds to the ferrimagnetic resonance losses. Dimri et al. [37] observed similar type of magnetic loss peak at a particular frequency due to resonance phenomenon. At resonance, oscillational frequency of domain walls matches well with the applied frequency.

3.7. Electrical properties

Fig. 10 shows dielectric constant versus frequency plots for the samples sintered at different sintering temperatures. It can be seen that like all other ferrite materials, the samples show frequency dependant phenomenon i.e. dielectric constant decreases with increasing frequency exhibiting normal ferrimagnetic behavior [38]. The simplest relation between dielectric constant and angular frequency ω is

$$\epsilon' = \frac{4\Pi\sigma'_{AC}}{\omega tan\delta}$$

where σ_{AC} is the ac conductivity, ω is the angular frequency and tanδ is the dielectric loss factor.

The mechanism of dielectric polarization in ferrites is similar to conduction mechanism. The electron exchange through $Fe^{2+} \leftrightarrow Fe^{3+}$ hopping mechanism results in local displacement of the electrons in the direction of applied electric field thereby polarization is induced in the ferrites [39]. In the present case, the dielectric constant is observed to be increasing with increasing sintering temperature. This is due to accelerated grain growth and improved hopping mechanism due to

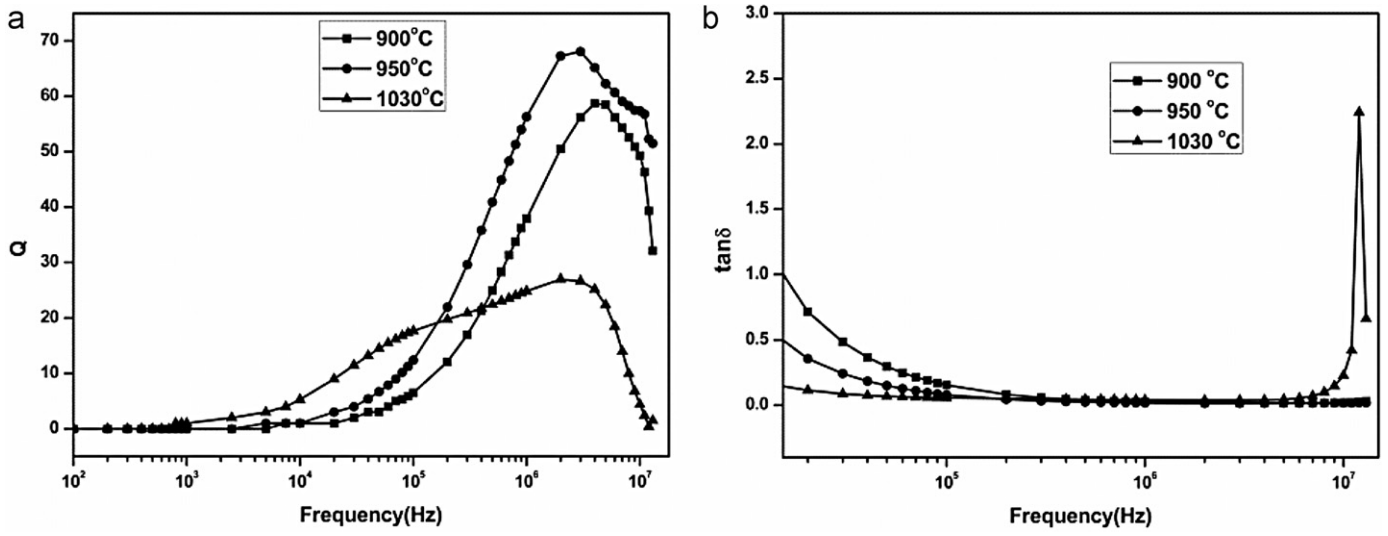

Fig. 9. (a) Quality factor (Q) and (b) magnetic loss factor (tanδ) versus frequency for $Ni_{0.50}Cu_{0.05}Zn_{0.45}Fe_2O_4$. ferrite sintered at 900 °C,950 °C and 1030 °C.

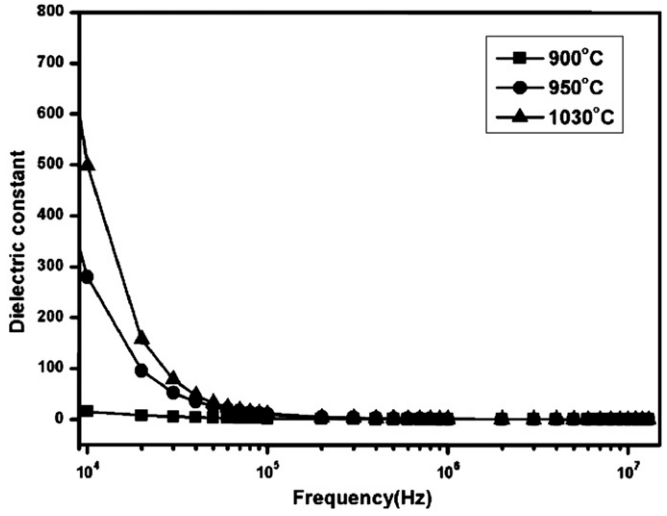

Fig. 10. Variation of dielectric constant with frequency for $Ni_{0.50}Cu_{0.05}Zn_{0.45}Fe_2O_4$ ferrite sintered at 900 °C,950 °C and 1030 °C.

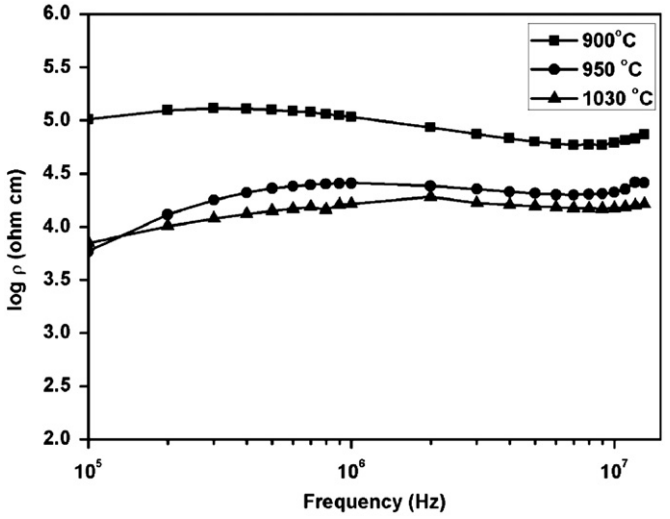

Fig. 11. AC electrical resistivity versus frequency for $Ni_{0.50}Cu_{0.05}Zn_{0.45}Fe_2O_4$ ferrite sintered at 900 °C,950 °C and 1030 °C.

the generation of divalent iron (Fe^{2+}) ions at elevated sintering temperature. At higher frequency, dielectric constant remains constant due to the fact that beyond a certain frequency of external AC field, the electron exchange between Fe^{2+} and Fe^{3+} cannot follow the alternating field [38].

AC electrical resistivity showed decreasing trend with increasing frequency. As the applied frequency increased there is an increased probability for jumping of electron through Fe^{2+}/Fe^{3+} ions.AC electrical resistivity data (Fig. 11) showed decreasing trend with increasing sintering temperature, the reason being increased grain size as well as the increased number of Fe^{2+} ions at B sites. The increased concentration of Fe^{2+} ions induces electron hopping $Fe^{2+} \leftrightarrow Fe^{3+}$ at B sites thereby reducing resistivity. The inverse relationship of dielectric constant with square root of resistivity is evidenced through the observations.

4. Conclusions

NiCuZn nano ferrite is successfully prepared through sol–gel method using polyvinyl alcohol as a chelating agent and observations showed formation of spinel phase at low annealing (500 °C) temperature having fine spherical particles. The results showed that material properties are sensitive to microstructure and they are enhanced with increase of sintering temperature. All the sintered samples are in single phase cubic spinel structure with an improved grain size as a function of sintering temperature. The samples manifest good values of magnetization, low magnetic losses at higher frequencies and high frequency stability of permeability with cut off frequency around 30 MHz.

Acknowledgments

Authors wish to thank Prof. C. Bansal, Dean, School of Physics, University of Hyderabad (UOH), India for providing XRD and FESEM facility. Also, the authors would like to express their gratitude to Dr. G. Jagan Reddy and Dr. A.R. James, DMRL, Hyderabad; Prof. P. Sarah, Vardaman Engineering College, Hyderabad for providing magnetic measurements facility.

References

[1] M.A. Gabal, Y.M. Al Angari, S.S. Al-Juaid, A study on Cu substituted Ni–Cu–Zn ferrites synthesized using egg-white, Journal of Alloys and Compounds 492 (2010) 411–415.
[2] Xiwei Qi, Ji Zhou, Zhenxing Yue, Zhilun Gui, Longtu Li, Effect of Mn substitution on the magnetic properties of MgCuZn ferrites, Journal of Magnetism and Magnetic Materials 251 (2002) 316–322.
[3] M. Saidani, M.A.M. Gijs, High-quality radio-frequency inductors on silicon using a hybrid ferrite technology, Applied Physics Letters 84 (2004) 4496–4498.
[4] Huaiwu Hua Su, Xiaoli Zhang, Baoyuan Tang, Liu, Yulan Jin, High Q-factor NiCuZn ferrite with nanocrystalline ferrite particles and Co_2O_3 additives, Physica Status Solidi A 204 (2007) 576–580.
[5] H.U. Jun, Y.A.N. Mi, Preparation of high-permeability NiCuZn ferrite, Journal of Zhejiang University SCIENCE 6B (6) (2005) 580–583.
[6] S.A. Ghodake, U.R. Ghodake, S.R. Sawant, S.S. Suryavanshi, P.P. Bakare, Magnetic properties of NiCuZn ferrites synthesized by oxalate precursor method, Journal of Magnetism and Magnetic Materials 305 (2006) 110–119.
[7] Feng Liu, Tianling Ren, Chen Yang, Litian Liu, A.Z. Wanga, Jun Yu, NiCuZn ferrite thin films for RF integrated inductors, Materials Letters 60 (2006) 1403–1406.
[8] Sea-Fue Wang, Yuh-Ruey Wang, Thomas C.K. Yang, Che-Fu Chen, Chun-An Lu, Chi-Yuen Huang, Densification and magnetic properties of low-fire NiCuZn ferrites, Journal of Magnetism and Magnetic Materials 220 (2000) 129–138.
[9] Yao Li, Jiupeng Zhao, Jiecai Han, Xiaodong He, Combustion synthesis and characterization of NiCuZn ferrite powders, Materials Research Bulletin 40 (2005) 981–989.
[10] M.A. Gabal n, Y.M. AlAngari, Low-temperature synthesis of nanocrystalline NiCuZn ferrite and the effect of Cr substitution on its electrical properties, Journal of Magnetism and Magnetic Materials 322 (2010) 3159–3165.
[11] J. Murbe, J. Topfer, Ni–Cu–Zn Ferrites for Low Temperature Firing: II. Effects of powder mopphology and Bi_2O_3 addition on microstructure and permeability, Journal of Electroceramics 16 (2006) 199–205.
[12] Ke Sun, Zhongwen Lan, Zhong Yu, Xiaona Jiang, Jiaomin Huang, Phase formation, grain growth and magnetic properties of NiCuZn ferrites, Journal of Magnetism and Magnetic Materials 323 (2011) 927–932.
[13] O.F. Caltun, L. Spinu, Al. Stancu, L.D. Thung, W. Zhou, Study of the microstructure and of the permeability spectra of Ni–Zn–Cu ferrites, Journal of Magnetism and Magnetic Materials 242–245 (2002) 160–162.
[14] M. Penchal Reddy, G. Balakrishnaiah, W. Madhuri, M. Venkata Ramana, N. Ramamanohar Reddy, K.V. Siva Kumar, V.R.K. Murthy, R. Ramakrishna Reddy, Structural, magnetic and electrical properties of NiCuZn ferrites prepared by microwave sintering method suitable for MLCI applications, Journal of Physics and Chemistry of Solids 71 (2010) 1373–1380.
[15] Su Hua, Zhang Huaiwu, Tang Xiaoli, Jing Yulan, Effects of calcing temperature and heating rate on properties of high-permeability NiCuZn Ferrites, Journal Magnetism and Magnetic Materials 302 (2006) 278–281.
[16] Chul Won Kim, Jae Gui Koh, A study of synthesis of NiCuZn-ferrite sintering in low temperature by metal nitrates and its electromagnetic property, Journal Magnetism and Magnetic Materials 257 (2003) 355–368.
[17] K. Venkateshwar Rao, C.S. Sunandana, XRD, microstructural and EPR susceptibility characterization ofcombustion synthesized nanoscale $Mg_{1-x}Ni_xO$ solid solutions, Journal of Physics and Chemistry of Solids 69 (2008) 87–96.
[18] K. Venkateswarlu, A. Chandra Bose, N. Rameshbabu, X-ray peak broadening studies of nanocrystalline hydroxyapatite by Williamson–Hall analysis, Physica B 405 (2010) 4256–4261.
[19] Ch. Sujatha, K. Venugopal Reddy, K. Sowri Babu, A. RamaChandra Reddy, K.H. Rao, Structural and Magnetic properties of Mg substituted NiCuZn Nano Ferrites, Physica B 407 (2012) 1232–1237.
[20] P.K. Roy, J. Bera, Effect of Mg substitution on electromagnetic properties of $(Ni_{0.25}Cu_{0.20}Zn_{0.55})$ Fe_2O_4 ferrite prepared by auto combustion method, Journal of Magnetism and Magnetic Materials 298 (2006) 38–42.
[21] V. Musat Bujoreanu, E. Segal, DSC study of water elimination from the coprecipitated ferrite powders, Journal of Thermal Analysis and Calorimetry 68 (2002) 191–197.
[22] S. Modak, M. Ammar, F. Mazaleyrat, S. Das, P.K. Chakrabarti, XRD, HRTEM and magnetic properties of mixed spinel nanocrystalline Ni–Zn–Cu-ferrite, Journal of Alloys and Compounds 473 (2009) 15–19.
[23] J. Kalarus, G. Kogias, D. Holz, V.T. Zaspalis, High permeability-high frequency stable MnZn ferrites, Journal of Magnetism and Magnetic Materials 324 (2012) 2788–2794.
[24] Muthafar F. Al-Hilli, Sean Li, Kassim D. Kassim, Gadolinium substitution and sintering temperature dependent electronic properties of Li–Ni ferrite, Materials Chemistry and Physics 128 (2011) 127–132.
[25] Jong-Gyu Paik, Man-Jong Lee, Sang-HooN Hyun, Reaction kinetics and formation of magnesium ferrites, Thermochimica Acta 425 (2005) 131–136.
[26] R.D. Waldron, Infrared spectra of Ferrites, Physical Review 99 (1955) 1727–1735.
[27] B.K. Labde, Madan C. Sable, N.R. Shamkwar, Structural and infrared studies of $Ni_{1+x}Pb_xFe_{2-2x}O_4$ system, Materials Letters 57 (2003) 1651–1655.
[28] T.K. Pathak, N.H. Vasoya, V.K. Lakhani, K.B. Modi, Structural and magnetic phase evolution study on needle-shaped nanoparticles of magnesium ferrite, Ceramics International 36 (2010) 275–281.
[29] A.I. Vogel, A Text book of Quantitative Inorganic Analysis, Third edition, Longman, London, 1975.
[30] M.A. Gabal, Effect of Mg substitution on the magnetic properties of NiCuZn ferrite nanoparticles prepared through a novel method using egg white, Journal of Magnetism and Magnetic Materials 321 (2009) 3144–3148.
[31] B. Parvatheeswara Rao, P.S.V. Subba Rao, K.H. Rao, Densification, grain growth and microstructure of Ni–Zn ferrites, Journal De Physique Iv (1997) 241–242.
[32] Ch. Sujatha, K. Venugopal Reddy, K. Sowri Babu, A. RamaChandra Reddy, K.H. Rao, Effects of heat treatment conditions on the structural and magnetic properties MgCuZn nano ferrites, Ceramics International 38 (2012) 5813–5820.
[33] T. Nakamura, Low-temperature sintering of Ni–Zn–Cu ferrite and its permeability spectra, Journal of Magnetism and Magnetic Materials 168 (1997) 285–291.
[34] M.R. Barati, Characterization and preparation of nanocrystalline MgCuZn ferrite powders synthesized by sol–gel auto-combustion method, Journal of Sol–Gel Science and Technology 52 (2009) 171–178.
[35] G. Herrera, Domain wall dispersions: relaxation and resonance in Ni–Zn ferrite doped with V_2O_5, Journal of Applied Physics 108 (2010) 103901.

[36] M. Manjurul Haque, M. Huq, M.A. Hakim, Influence of CuO and sintering temperature on the microstructure and magnetic properties of Mg–Cu–Zn ferrites, Journal of Magnetism and Magnetic Materials 320 (2008) 2792–2799.

[37] Mukesh C. Dimri, A. Verma, Subhash C. Kashyap, D.C. Dube, O.P. Thakur, Chandra Prakash, Structural, dielectric and magnetic properties of NiCuZn ferrite grown by citrate precursor method, Materials Science and Engineering: B 133 (2006) 42–48.

[38] E. Melagiriyappa, H.S. Jayannaa, B.K. Chougule, Dielectric behavior and ac electrical conductivity study of Sm^{3+} substituted Mg–Zn ferrites, Materials Chemistry and Physics 112 (2008) 68–73.

[39] B. Parvatheeswara Rao, K.H. Rao, Effect of sintering conditions on resistivity and dielectric properties of Ni–Zn ferrites, Journal of Materials Science 32 (1997) 6049–6054.